Biophysical Chemistry, 39 (1991) 241–251

BIOCHE 01543

Anisotropy decays of indole, melittin monomer and melittin tetramer by frequency-domain fluorometry and multi-wavelength global analysis

Joseph R. Lakowicz, Ignacy Gryczynski, Henryk Cherek and Gabor Laczko

University of Maryland at Baltimore, Center for Fluorescence Spectroscopy and School of Medicine, Department of Biological Chemistry, 660 West Redwood Street, Baltimore, MD 21201, U.S.A.

Received 24 April 1990
Revised manuscript received 2 October 1990
Accepted 3 October 1990

Frequency-domain fluorometry; Anisotropy decay; Multi-wavelength global analysis; Indole; Melittin; Rotational diffusion

We used frequency-domain fluorescence spectroscopy to measure the fluorescence lifetime and anisotropy decays of indole in propylene glycol, and of the tryptophan emission of melittin monomer and tetramer in water solutions at 5 °C. We obtained an increase in resolution of the anisotropy decays by using multiple excitation wavelengths, chosen to provide a range of fundamental anisotropy values. The multi-excitation wavelength anisotropy decays were analyzed globally to recover a single set of correlation times with wavelength-dependent anisotropy amplitudes. Simulated data and χ^2_R surfaces are shown to reveal the effect of multi-wavelength data on the resolution of complex anisotropy decays. For both indole and melittin, the anisotropy decays are heterogeneous and require two correlation times to fit the frequency-domain data. For indole in propylene glycol at 5 °C we recovered correlation times of 0.59 and 4.10 ns, which appear to be characteristic of the rigid and asymmetric indole molecule. For melittin monomer the correlation times were 0.13 and 1.75 ns, and for melittin tetramer 0.12 and 3.96 ns. The shorter and longer correlation times of melittin are due to segmental motions and overall rotational diffusion of the polypeptide.

1. Introduction

Fluorescence anisotropy decays of rigid molecules provide information on the size and shape of the molecules, and on the interactions of fluorophores with solvent molecules [1–4]. Recently, Fleming et al. [3,5] and Lakowicz et al. [6,7] measured and discussed slip and stick boundary conditions in the rotational hydrodynamics of rigid organic fluorophores. Complex phenomena also govern the anisotropy decays of biological macromolecules. In addition to slip and stick diffusive motions of the fluorophores, the anisotropy decays are influenced by segmental motions of the polypeptide backbone and overall rotational diffusion of the proteins. Consequently, the anisotropy data provide the same information as for rigid molecules, but can also reveal the extent of segmental flexibility [8–10]. For a rigid spherical molecule (few, if any, macromolecules are rigid and spherical) the anisotropy decays as a single exponential. Multiexponential anisotropy decays are expected for asymmetric proteins [11,12] and asymmetric aromatic molecules [13–15]. Still more complex anisotropy decays are expected for hindered probes in membranes and for macromolecules with segmental flexibility [16,17]. The main difficulty in the use of anisotropy decays is obtaining adequate data to recover closely spaced rotational correlation times. This difficulty is due to the subnanosecond time scale of many rota-

Correspondence address: J.R. Lakowicz, University of Maryland at Baltimore, Center for Fluorescence Spectroscopy and School of Medicine, Department of Biological Chemistry, 660 West Redwood Street, Baltimore, MD 21201, U.S.A.

tional processes, and the need to perform accurate anisotropy measurements on this time scale.

In the present paper we report the resolution of two correlation times which describe the anisotropy decays of indole and melittin. We obtained improved resolution of the multiple correlation times by two means. Firstly, anisotropy data were obtained in the frequency domain [18,19] which is now known to provide good resolution of rapid and/or complex anisotropy decays [20–22]. Secondly, the data were obtained at several excitation wavelengths at which the fundamental anisotropies (r_0) are distinct, followed by global analysis to recover a single set of correlation times. It is known that for different values of r_0 the various correlation times contribute differently to the anisotropy data [23,24] because of the changing position of the transition moments relative to the molecular axes. Additionally, we described simulated data to illustrate the form of the data, and the effect of multi-wavelength data on the resolution of closely spaced correlation times.

2. Theory

The anisotropy decay at each excitation wavelength (λ) can be described by a sum of exponentials,

$$r^{\lambda}(t) = \sum_i r_0^{\lambda} g_i \exp(-t/\theta_i) \tag{1}$$

where r_0^{λ} is the limiting anisotropy at λ and θ_i are the correlation times. The value of $r_0^{\lambda} g_i$ represents the amplitude of the anisotropy which decays via the i-th correlation time. In the present paper we assumed during the analysis that the value of r_0^{λ} was not known, so that the variable amplitude is given by the product. Hence, there are i variable amplitudes ($r_0^{\lambda} g_i$) for each excitation wavelength. This representation is convenient in that the value of $r_0^{\lambda} g_i$ is sometimes known. In this case the variable becomes g_i with $\Sigma_i g_i = 1.0$. It should be noted that the correlation times are related, but not equal to, the rotational diffusion coefficients of the fluorophore about the principle axes [1,8,12]. The value of r_0^{λ} depends upon the angle between the absorption and emission transition moments at each excitation wavelength. This dependence in turn alters the relative contribution of each rotational motion to the anisotropy data.

In the frequency domain the measured values are the phase angle difference between the parallel ($\|$) and perpendicular ($\perp$) components of the fluorescence ($\Delta_{\omega}^{\lambda} = \phi_{\perp} - \phi_{\|}$) and the ratio of the polarized and modulated components of the emission ($\Lambda_{\omega}^{\lambda} = m_{\|}/m_{\perp}$), each measured over a range of modulation frequencies (ω). The parallel and perpendicular components of the emission are given by

$$I_{\|}^{\lambda}(t) = \tfrac{1}{3} I_0^{\lambda}(t)\left[1 + 2r^{\lambda}(t)\right] \tag{2}$$

$$I_{\perp}^{\lambda}(t) = \tfrac{1}{3} I_0^{\lambda}(t)\left[1 - r^{\lambda}(t)\right] \tag{3}$$

where $I_0(t)$ is the decay of the total emission. Calculated values ($\Delta_{c\omega}$ and $\Lambda_{c\omega}$) are obtained using

$$\Delta_{c\omega}^{\lambda} = \arctan\left(\frac{D_{\|}^{\lambda} N_{\perp}^{\lambda} - N_{\|}^{\lambda} D_{\perp}^{\lambda}}{N_{\|}^{\lambda} N_{\perp}^{\lambda} + D_{\|}^{\lambda} D_{\perp}^{\lambda}}\right) \tag{4}$$

$$\Lambda_{c\omega}^{\lambda} = \left(\frac{\left(N_{\|}^{\lambda}\right)^2 + \left(D_{\|}^{\lambda}\right)^2}{\left(N_{\perp}^{\lambda}\right)^2 + \left(D_{\perp}^{\lambda}\right)^2}\right)^{1/2} \tag{5}$$

where

$$N_i^{\lambda} = \int_0^{\infty} I_i^{\lambda}(t) \sin \omega t \, dt \tag{6}$$

$$D_i^{\lambda} = \int_0^{\infty} I_i^{\lambda}(t) \cos \omega t \, dt \tag{7}$$

and i represents parallel or perpendicular. Frequency-domain data were obtained at several excitation wavelengths and were analyzed to recover one or two correlation times by the method of nonlinear least-squares [25,26]. The goodness-of-fit is estimated from the value of reduced chi-squared

$$\chi_R^2 = \frac{1}{\nu} \sum_{\omega,\lambda} \left(\frac{\Delta_{\omega}^{\lambda} - \Delta_{c\omega}^{\lambda}}{\delta\Delta_{\omega}}\right)^2 + \frac{1}{\nu} \sum_{\omega,\lambda} \left(\frac{\Lambda_{\omega}^{\lambda} - \Lambda_{c\omega}^{\lambda}}{\delta\Lambda_{\omega}}\right)^2 \tag{8}$$

where ν is the number of degrees of freedom, and $\delta\Delta_{\omega}$ and $\delta\Lambda_{\omega}$ denote the uncertainties in the measured quantities. For both simulations and analy-

sis the uncertainties were assumed to be $\delta\Delta = 0.2°$ and $\delta\Lambda = 0.005$, independent of the modulation frequency.

The modulation ratio Λ_ω can be presented in modified form as the modulated anisotropy

$$r_\omega^\lambda = \left(\Lambda_\omega^\lambda - 1\right)/\left(\Lambda_\omega^\lambda + 2\right) \qquad (9)$$

At low modulation frequencies r_ω^λ is nearly equal to r^λ (the steady-state anisotropy). At high modulation frequencies r_ω^λ approaches r_0^λ (the fundamental anisotropy).

3. Materials and methods

Indole was recrystallized from petroleum ether. Melittin (from Serva Fine Biochemicals, Garden City Park, NY, cat. no. 51560) is claimed to be pure by high-performance liquid chromatography (HPLC) and free of *N*-formylmelittin. Examination of solvents (propylene glycol or the buffer, 10 mM Tris, pH 7) revealed no significant fluorescence or scatter at any of the excitation wavelengths. Frequency-domain data were obtained on the instrument described previously [19], modified as follows. To obtain suitable wavelengths for excitation at and below 300 nm, this instrument was equipped with a continuous ultraviolet laser light source. This source consisted of an argon ion laser (Coherent, Innova 15) and a ring dye laser (model 699). The dye was rhodamine 6G. Continuous ultraviolet radiation is obtained from a temperature tuned doubling crystal KDP. This ultraviolet radiation was then modulated using a Lasermetrics 1042 electro-optic modulator. The emission was observed through a WG 320 filter.

4. Results

4.1. Stimulations for a rigid rotator

Rigid, nonspherical molecules can display multiexponential anisotropy decays. We estimated the effects of global analysis of the multi-wavelength data and global analysis on the resolution of closely spaced correlation times by the use of

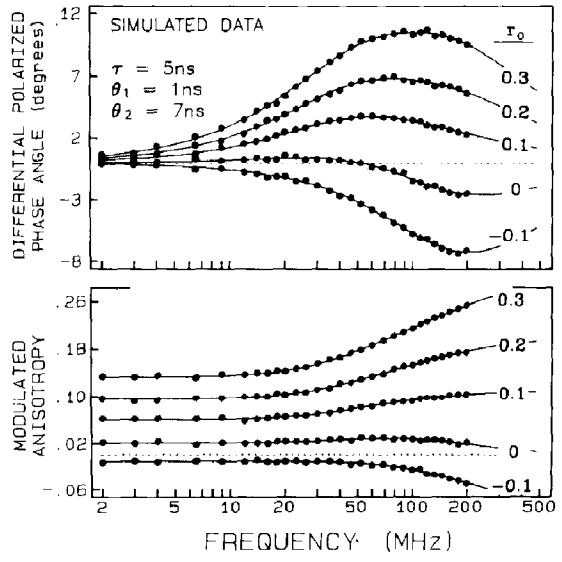

Fig. 1. Simulated differential phase and modulated anisotropy data for a rigid nonspherical molecule. The assumed parameter values are shown.

simulated frequency-domain data. The frequency range of the simulations was from 2 to 200 MHz, the upper frequency being the practical limit of the electro-optic modulation and detector use in this configuration of our frequency-domain fluorometer [19]. Data were simulated using an assumed single-exponential lifetime of 5 ns, and correlation times of 1 and 7 ns. Five different r_0 values were assumed, ranging from 0.3 to -0.1 (fig. 1). This ratio of correlation times is expected for small disc-like molecules and can be considered representative of the out-of-plane and in-plane rotations in solutions of modest viscosity. Examination of the simulated data shows that the differential phase angles are strongly dependent upon r_0, and that the values of Δ_ω become negative for negative r_0 values. Interestingly, nonzero values of Δ_ω, both positive and negative, are found when $r_0 = 0.0$. This can only occur for an asymmetrically rotating molecule, as was first pointed out by Weber [31] for the temperature dependence of the steady-state anisotropy. The observation of nonzero differential phase angles at $r_0 = 0$ can be regarded as proof of more than one rate of rotational diffusion. A similar effect $r_0 = 0$ is seen for

the modulated anisotropies (fig. 1, lower panel), except that it appears that higher frequency data are needed to observe the change in values of r_ω from positive to negative.

Table 1 shows the results of global analysis of simulated data for five wavelengths or r_0 values. The recovered amplitudes and correlation times are in excellent agreement with the assumed values. The single-correlation-time fit gives an unacceptably high value of $\chi^2_R = 133.1$, whereas the global fit yields $\chi^2_R = 1.10$.

We questioned the uncertainties in the recovered correlation times and amplitudes in the case of multi-wavelength and single-wavelength simulated data. We examined the values χ^2_R as each correlation time was varied about the value yielding the χ^2_R minimum (fig. 2). Using this fixed value the least-squares analysis was performed again, allowing the remaining correlation times and all the amplitudes to vary, yielding the minimum value of χ^2_R consistent with the fixed correlation time. Since all the other parameters vary during reanalysis, this procedure should account for all correlations between the parameter values. This computation was performed for both the single- (top) and multi-wavelength (bottom) simulated data. The uncertainty in the correlation times depends upon the r_0 value. The best resolution (lowest uncertainty) is obtained at the highest r_0 value. For global analysis (fig. 2, bottom) the uncertainty is about 50% lower than for the best single (highest r_0) file. The dashed line in fig. 2 indicates the value of χ^2_R expected 33% of the time due to random errors in the data. For lack of a rigorous theory for uncertainties, we take this

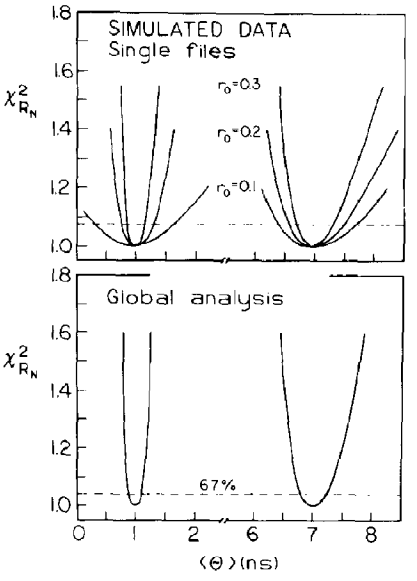

Fig. 2. Correlation time χ^2_R surfaces for simulated frequency-domain anisotropy data for a rigid rotator (fig. 1). (Top) Single-wavelength (single r_0) data. (Bottom) Global analysis for five r_0 values. The dashed lines indicate the value of χ^2_R expected 67% of the time due to random errors in the data.

elevation in χ^2_R as defining the uncertainty in the correlation times. The effect of global analysis of multi-wavelength data is both to sharpen the χ^2_R surface, and to increase the significance of the elevated χ^2_R due to the increased number of data points. Given the difficulty of obtaining the multi-wavelength data, the increase in resolution, above that which is obtainable from the single best (highest r_0) file, is modest. Hence, this procedure is probably only justified for the most critical

Table 1

Global analysis of simulated frequency-domain anisotropy data, with a single-exponential intensity decay $\tau = 5$ ns and a double-exponential anisotropy decay with correlation times of 1 and 7 ns

r_0^λ	Assumed		Recovered		θ_1 (ns)	θ_2 (ns)	χ^2_R
	$r_0^\lambda g_1$	$r_0^\lambda g_2$	$r_0^\lambda g_1$	$r_0^\lambda g_2$			
0.3	0.10	0.20	0.099	0.199	1.02	7.00	1.10
0.2	0.05	0.15	0.049	0.150			
0.11	0.01	0.10	0.010	0.101			
0.0	−0.05	0.05	−0.05	0.05			
−0.03	−0.10	0.01	−0.10	0.011			
One correlation time fit					4.32	–	133.1

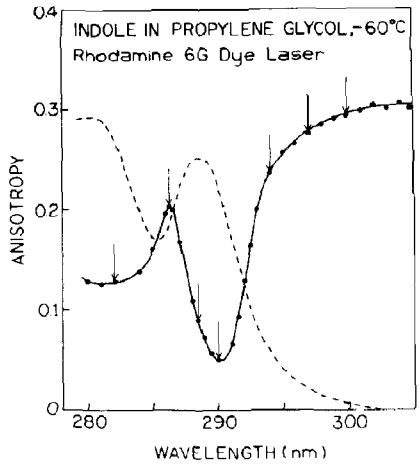

Fig. 3. Anisotropy (—) and absorption (---) spectra of indole in propylene glycol at −60 °C. The arrows indicate excitation wavelengths, used for collecting the frequency-domain anisotropy data.

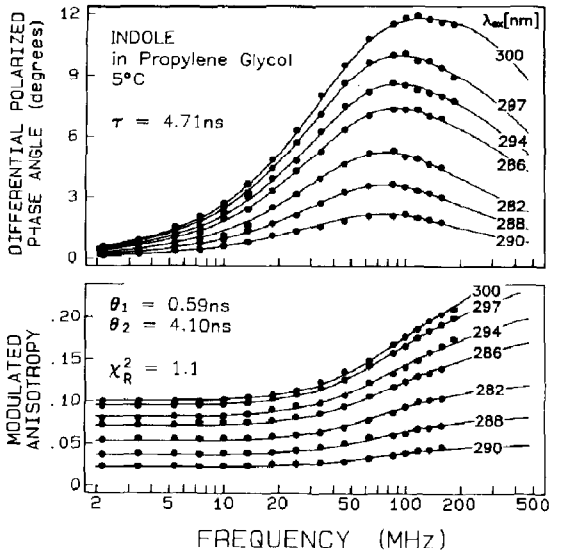

Fig. 4. Differential phase and modulated anisotropy data for indole in propylene glycol at 5 °C. The excitation wavelengths are shown.

applications, for which a range of suitable wavelengths (r_0 values) is available and for which one requires the maximum possible resolution of the correlation times.

4.2. Indole in propylene glycol

Indole is a useful test compound for the resolution of complex anisotropy decays. Indole is asymmetric and most probably displays different rotational rates about each molecular axis. Additionally, the well-known presence of two electronic transitions (^1L_a and ^1L_b) results in an anisotropy spectrum which is strongly dependent upon the excitation wavelength (fig. 3). These steady-state anisotropies were obtained using the ring dye laser as the excitation source, without any intensity modulation. The arrows indicate the wavelengths chosen for collection of the frequency-domain anisotropy data. The wavelengths provide r_0^λ values ranging from 0.296 to 0.051. The intensity decays of indole in propylene glycol at 5 °C (not shown) were found to be essentially independent of the excitation wavelength, and very

Table 2

Global analysis of frequency-domain anisotropy data for indole in propylene glycol at 5 °C

λ_{exc} (nm)	r_0^λ	$r_0^\lambda g_1$	$r_0^\lambda g_2$	θ_1 (ns)	θ_2 (ns)	χ^2_R
300	0.296 [a]	0.104	0.190	0.59	4.10	1.1
297	0.275	0.063	0.189			
294	0.237	0.050	0.163			
286	0.203	0.040	0.142			
282	0.130	0.014	0.111			
288	0.088	0.007	0.077			
290	0.051	0.002	0.048			
One correlation time fit				3.10	–	18.8

[a] From the anisotropy spectrum at −60 °C (fig. 3).

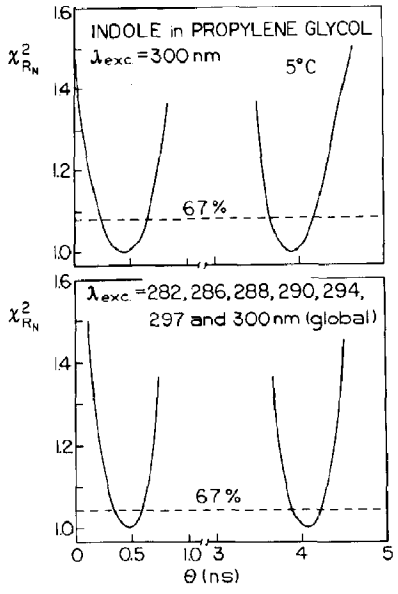

Fig. 5. Correlation time χ^2_R surfaces for indole in propylene glycol at 5 °C. (Top) Single-wavelength data (with highest r_0). (Bottom) Global analysis for five excitation wavelengths. The dashed lines indicate the value of χ^2_R expected 67% of the time due to random errors.

close to a single-exponential decay under our experimental conditions. We used an average value of 4.71 ns.

Differential phase and modulated anisotropy data for indole in propylene glycol at 5 °C are presented in fig. 4. Two correlation times are needed to fit data, 0.59 and 4.10 ns (table 2). It was not possible to fit the data using a single correlation time, and this attempt resulted in an 18-fold increase in χ^2_R. The recovered anisotropy amplitudes were found to be strongly dependent upon the excitation wavelength. Importantly, the sum of the amplitudes at each wavelength agreed with the fundamental anisotropy at this wavelength (table 2).

The correlation time χ^2_R surfaces for the correlation times of indole in propylene glycol are shown in fig. 5. As predicted by the simulations, there is an approx. 50% reduction in the uncertainties resulting from global analysis of data obtained at seven excitation wavelengths. The uncertainties from the global analysis are about 0.2 and 0.3 ns for shorter and longer correlation times, respectively. Once again we note that a single measurement at the highest value of r_0 is an efficient way to recover the correlation times for an asymmetric molecule.

4.3. Simulations for a flexible peptide

It is interesting to simulate the frequency-domain data expected for a flexible protein. Most proteins display nonexponential intensity decays [27–30], and hence we chose a double-exponential decay with decay times 0.8 and 4 ns and amplitudes of 0.5 each. Due to segmental motions of short regions of the peptide, and torsional motions of the indole ring, protein anisotropy decays may display short components in the range of tens to hundreds of picoseconds. For the simulations we chose two correlation times of 0.1 and 4 ns. The

Table 3

Global analysis data for simulated (protein-like) anisotropy data with a double-exponential intensity decay [a] ($\tau = 0.8$ and 4 ns, $\alpha_1 = \alpha_2$) and double-exponential anisotropy decay with 0.1 and 4 ns

r_0^λ	Assumed		Recovered		θ_1 (ns)	θ_2 (ns)	χ^2_R
	$r_0^\lambda g_1$	$r_0^\lambda g_2$	$r_0^\lambda g_1$	$r_0^\lambda g_2$			
0.3	0.16	0.14	0.163	0.141	0.09	3.95	1.0
0.24	0.12	0.12	0.129	0.120			
0.18	0.08	0.10	0.083	0.101			
0.12	0.04	0.08	0.035	0.081			
0.07	0.01	0.06	0.007	0.060			
One correlation time fit					3.05	–	7.8

[a] The intensity decay is given by $I(t) = \Sigma_i \alpha_i e^{-t/\tau_i}$.

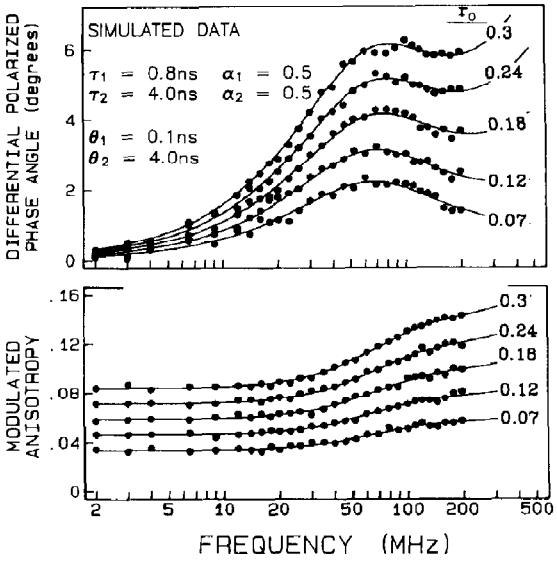

Fig. 6. Simulated differential phase and modulated anisotropy data using parameters expected for a flexible peptide. The assumed correlation times for segmental motions of the fluorophore and for overall rotational diffusion are 0.1 and 4.0 ns, respectively.

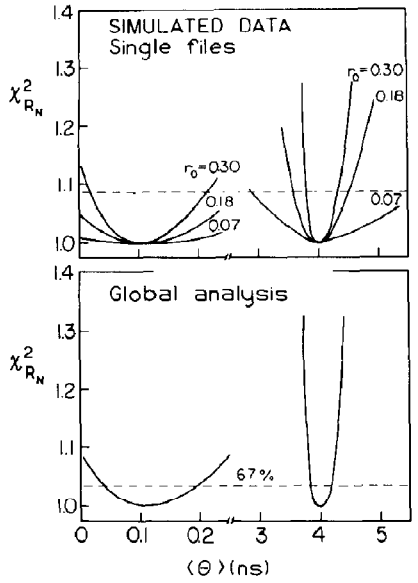

Fig. 7. Correlation time χ^2_R surfaces for simulated data for a flexible peptide. (Top) Single-wavelength files. (Bottom) Global analysis. The dashed lines indicate the value of χ^2_R expected 67% of the time due to random errors.

limiting anisotropy was chosen to be comparable to that of tryptophan, and we chose five values from 0.3 to 0.07. The files were analyzed individually and globally (table 3). Fig. 6 shows the differential phase and modulated anisotropy data, as well as the global fit to these data. For modulation frequencies higher than 200 MHz the short components in the anisotropy decay dominate the differential phase angles. This is especially apparent for the high r_0^λ values where the simulated curves increase rapidly above 200 MHz (fig. 6). The two correlation times obtained from global analysis were in agreement with the simulated values, as were the r_0^λ values. The single-correlation-time fit resulted in a 7.8-fold increase in χ^2_R as compared to the two-component fit. The χ^2_R surfaces for the single file and global fits are presented in fig. 7. It should be noted that for excitation with r_0^λ lower than 0.2 it is difficult to recover the shorter correlation time, especially if the data are obtained for a single excitation wavelength. Hence, if one wishes to measure correlation times nonglobally, then the excitation wavelength should be chosen carefully, and preferably at the value yielding the highest value of r_0^λ.

4.4. *Melittin monomer and tetramer*

Melittin provides a useful protein to test the concept of multiexcitation wavelength anisotropy data. Melittin contains a single tryptophan residue, and no tyrosine residues, so that one can exclude energy transfer as a contributor to the anisotropy decay. Additionally, melittin can exist in a monomeric random-coil state at low ionic strength, or as an α-helical tetramer at high ionic strength, and one expects different anisotropy decays from this distinct form.

Fig. 8 shows the steady-state anisotropy spectra of melittin monomer and tetramer in a mixture of propylene glycol and water (70 : 30) at $-60\,^\circ$C. The arrows show the excitation wavelengths used for the frequency-domain experiments. Under these conditions, there is no diffusive motion, so that the measured anisotropies are expected to be the fundamental anisotropies. Except for the red-edge region of the spectra, the r_0 values for melittin tetramer are slightly lower than for melittin

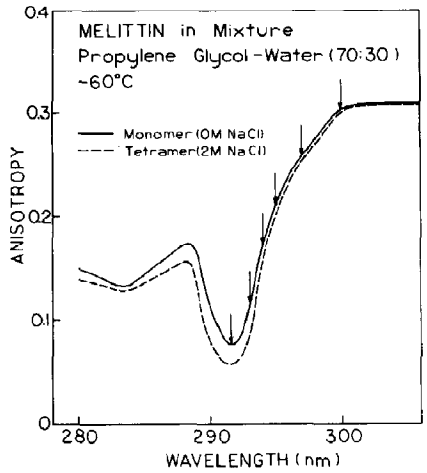

Fig. 8. Anisotropy spectra for melittin in mixture of propylene glycol-water (70:30) at −60°C. The arrows indicate excitation wavelengths.

monomer. This result is consistent with energy migration between the tryptophan residues in the tetramer, assuming the protein remains in the tetrameric state in the propylene glycol-water mixture. The apparent absence of energy transfer at 300 nm excitation is in agreement with previous studies, which interpret this red-edge effect as being due to an unusual electronic transition [32]. This phenomenon is now thought to be due to the decreased spectral overlap resulting from red-edge excitation shifts [33–36]. It is difficult to be certain with regard to the possibility of energy transfer between the tryptophan residues. The Förster distance for indole-indole transfer in cyclohexane is 14.8 Å [37]. This distance is comparable to the distance between the tryptophan residues in melittin tetramer, which are 8 and 27 Å for the more closely spaced and more distant pairs in the tetramer [38]. However, the Förster distance for indole-indole transfer in protic solvents, where the Stokes' shift is larger, is near 4Å [38], so that little energy transfer is expected. In any event, the differences in the anisotropy spectra of melittin monomer and tetramer are small, so that Trp-Trp energy transfer does not appear to contribute significantly to the anisotropy decay.

The fluorescence intensity decays of melittin monomer and tetramer show no significant dependence on excitation wavelength. Table 4 contains data obtained from multiexponential analysis of intensity decays for melittin monomer and tetramer. Three decay times are needed to fit the data in both states.

Table 4

Multiexponential intensity decay analysis of melittin monomer and tetramer at 5°C

	τ_i (ns)	α_i	f_i	χ^2_R
Melittin monomer	3.46	1	1	156.7
	1.20	0.399	0.149	
	4.57	0.601	0.851	3.2
	0.24	0.343	0.032	
	2.58	0.374	0.377	
	5.35	0.283	0.591	1.1
Melittin tetramer (2 M NaCl)	2.67	1	1	167.6
	1.18	0.519	0.244	
	3.94	0.981	0.756	3.7
	0.31	0.341	0.050	
	2.33	0.497	0.553	
	5.15	0.161	0.397	1.4

Figs 9 and 10 show frequency-domain anisotropy data for melittin monomer and tetramer,

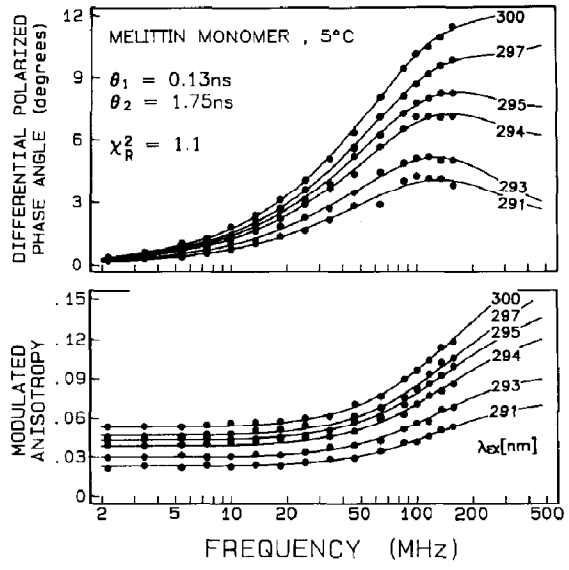

Fig. 9. Differential phase and modulated anisotropy data for melittin monomer.

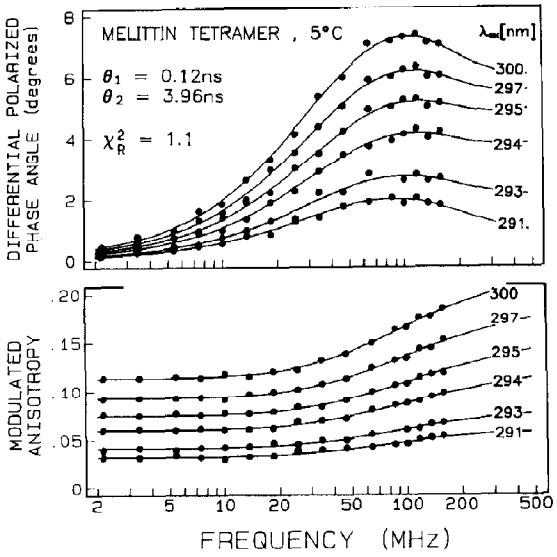

Fig. 10. Differential phase and modulated anisotropy data for melittin tetramer.

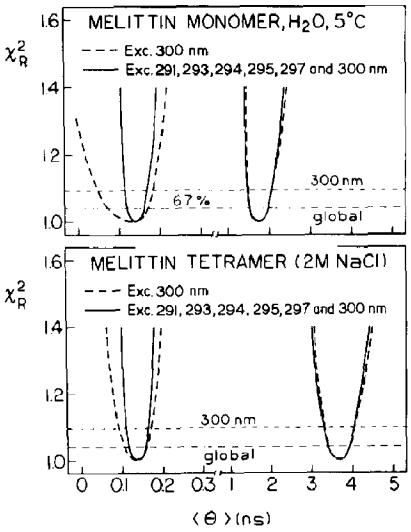

Fig. 11. Correlation time χ^2_R surfaces for melittin. (Top) Melittin monomer. (Bottom) Melittin tetramer. The dashed lines indicate the values of χ^2_R expected 67% of the time due to random errors.

respectively. In both cases two correlation times are needed to fit the experimental data. Anisotropy decay parameters recovered from global analysis (correlation times and amplitudes) for melittin are listed in table 5. In these analyses the total anisotropies (r_0^λ) were floating parameters.

For melittin tetramer the longer correlation time is 2.5-fold higher than for the monomer, which is consistent with the larger hydrodynamic size of the tetramer. The shorter correlation time of the tetramer is only slightly lower than that found for

Table 5

Global analysis data for anisotropy decay of melittin in 10 mM Tris (pH 7) at 5°C

λ_{exc} (nm)	r_0^λ [a]	$r_0^\lambda g_1$	$r_0^\lambda g_2$	θ_1 (ns)	θ_2 (ns)	χ^2_R
Melittin monomer						
300	0.305	0.188	0.136	0.13	1.75	1.1
297	0.258	0.150	0.121			
295	0.210	0.094	0.118			
294	0.172	0.071	0.107			
293	0.115	0.017	0.088			
291	0.082	0.019	0.067			
One correlation time fit				1.37	–	4.5
Melittin tetramer						
300	0.300	0.096	0.190	0.11	3.96	1.1
297	0.246	0.089	0.154			
295	0.200	0.082	0.123			
294	0.158	0.060	0.099			
293	0.086	0.029	0.069			
291	0.058	0.008	0.055			
One correlation time fit				3.22	–	3.8

[a] From the anisotropy spectrum at −60°C (fig. 8).

the monomer. The limiting anisotropies recovered from analysis ($\Sigma r_0^{\lambda} g_i$) are in relatively good agreement with measured values of r_0^{λ}. Fig. 11 shows the correlation time χ_R^2 surfaces for melittin monomer and tetramer, for the best single file and for global analyses. The global analysis yields about 20% less uncertainty for the longer correlation times, but shorter correlation times are significantly better estimated using global analysis.

5. Discussion

We used global analysis of simulated and experimental frequency-domain anisotropy data to recover multiple correlation times of asymmetric and/or flexible molecules. We examined two experimental cases; the anisotropic rotation of indole in propylene glycol and the segmental motions of melittin in the monomeric and the tetrameric states. In each case there are different origins for the multiexponential anisotropy decays. For indole in propylene glycol we obtained two correlation times, 0.59 and 4.1 ns; the shorter correlation time may be related to an in-plane rotation, and the longer correlation time to an out-of-plane rotation. It is also possible that rotational diffusion of indole in propylene glycol occurs with partial 'stick' and 'slip' boundary conditions, and that these processes contribute to the observed double-exponential anisotropy decay.

It seems likely that additional processes are responsible for the short and long correlation times of melittin. In both the monomer and the tetramer, the short correlation time is near 100 ps. This component is probably due to segmental motions of the tryptophan and the nearby amino acids. The correlation time for indole in water is near 50 ps [21], so that the indole torsional motions are only slightly slowed by the attached and/or adjacent peptide chain.

The data for melittin tetramer may be slightly distorted because of energy migration between the tryptophans. However, we believe that energy transfer plays an insignificant role in the anisotropy decay of melittin. Additionally, some excitation wavelengths were on the red edge of the anisotropy spectrum (fig. 8), where energy transfer is known to fail [32]. Additionally, we note that the multi-wavelength method is limited to proteins which lack tyrosine residues. If one or more tyrosine residues were present, then the shorter wavelength excitation would result in tyrosine excitation, with subsequent energy transfer to and depolarization of the tryptophan emission.

Finally, we note that the use of multiexcitation wavelengths resulted in only a modest increase in resolution of the correlation times. Given the increased time and difficulty of obtaining the data, such measurements are only justified in experimental situations which demand the highest attainable resolution. We previously described an alternative approach, in which the fluorescence lifetime is varied by collisional quenching [7,15,21] and/or energy transfer [6]. These processes decrease the mean decay time of the fluorophore, and thereby alter the contribution of each rotational motion to the anisotropy data. It is our opinion that the use of quenching, and global analysis of the anisotropy data from the quenched samples [6,7,15,21], is superior to the multi-wavelength measurements for enhanced resolution of multiple correlation times.

Acknowledgements

This work was supported by grants DMB-8804931, DMB-8502835 and DIR-8804831 from the National Science Foundation. J.R.L. and G.L. express appreciation for financial support from the Medical Biotechnology Center at the University of Maryland School of Medicine.

References

1 T.J. Chuang and K.B. Eisenthal, J. Chem. Phys. 57 (1972) 5094.
2 R.F. Steiner, Excited states of biopolymers (Plenum, New York, 1983) p. 117.
3 G.R. Fleming, Chemical applications of ultrafast spectroscopy (Oxford University Press, New York, 1986) Ch. 6.
4 J.R. Lakowicz, Principles of fluorescence spectroscopy (Plenum, New York, 1983).
5 G.R. Fleming, A.E.W. Knight, J.M. Morris, R.J. Robins and G.W. Robinson, Chem. Phys. Lett. 51 (1977) 399.

6 J.R. Lakowicz, I. Gryczynski and W. Wiczk, Chem. Phys. Lett. 149 (1988) 134.
7 J.R. Lakowicz, I. Gryczynski, W. Wiczk and M.L. Johnson, Biophys. Chem. 30 (1988) 271.
8 G.G. Belford, R.L. Belford and G. Weber, Proc. Natl. Acad. Sci. U.S.A. 69 (1972) 1392.
9 B.P. Maliwal and J.R. Lakowicz, Biochim. Biophys. Acta 873 (1986) 161.
10 J.R. Lakowicz, G. Laczko, I. Gryczynski and H. Cherek, J. Biol. Chem. 261 (1986) 2240.
11 G. Weber, Biochem. J. 51 (1952) 145.
12 E.W. Small and I. Isenberg, Biopolymers 16 (1977) 1907.
13 T. Tao, Biopolymers 8 (1969) 609.
14 G. Weber, J. Chem. Phys. 66 (1977) 4081.
15 I. Gryczynski, H. Cherek, G. Laczko and J.R. Lakowicz, Chem. Phys. Lett. 135 (1987) 193–199.
16 K. Kinosita, S. Kowata and A. Ikegami, Biophys. J. 20 (1977) 289.
17 G. Lapari and A. Szabo, Biophys. J. 30 (1980) 489.
18 E. Gratton and M. Limkeman, Biophys. J. 44 (1983) 315.
19 J.R. Lakowicz and B.P. Maliwal, Biophys. Chem. 21 (1985) 61.
20 B.P. Maliwal, A. Hermetter and J.R. Lakowicz, Biochim. Biophys. Acta 873 (1986) 173.
21 J.R. Lakowicz, H. Cherek, I. Gryczynski, N. Joshi and M.L. Johnson, Biophys. J. 51 (1987) 755.
22 J.R. Lakowicz, H. Szmacinski and I. Gryczynski, Photochem. Photobiol. 47 (1988) 31.
23 M.D. Barkley, A. Kowalczyk and L. Brand, J. Chem. Phys. 75 (1981) 3581.
24 I. Gryczynski, H. Cherek, G. Laczko and J.R. Lakowicz, Chem. Phys. Lett. 135 (1987) 193.
25 P.R. Bevington, Data reduction and error analysis for the physical sciences (McGraw-Hill, New York, 1969).
26 J.R. Lakowicz, H. Cherek, B.P. Maliwal and E. Gratton, Biochemistry 26 (1985) 376.
27 A.G. Szabo and D.M. Rayner, J. Am. Chem. Soc. 102 (1980) 554.
28 R.J. Robbins, G.R. Fleming, G.S. Beddard, G.W. Robinson, P.J. Thinthethwait and G.J. Wolfe, J. Am. Chem. Soc. 102 (1980) 6271.
29 J.M. Beechem and L. Brand, Annu. Rev. Biochem. 54 (1985) 43.
30 A. Grinvald and I.Z. Steinberg, Biochim. Biophys. Acta 427 (1976) 663.
31 G. Weber, J. Chem. Phys. 55 (1971) 2399.
32 G. Weber and M. Shinitzky, Proc. Natl. Acad. Sci. U.S.A. 65 (1970) 823.
33 K.I. Rudik and L.C. Pikulik, Opt. Spectrosc. 30 (1971) 147.
34 A.N. Rubinov and V.I. Tomin, Opt. Spectrosc. 29 (1970) 578.
35 I. Yu. Tekhves and V.V. Khizhnyakov, Soc. Phys. JETP 42 (1976) 305.
36 A.P. Demchenko, Ultraviolet spectroscopy of proteins (Springer, Berlin, 1986).
37 I.B. Berlman, Energy transfer parameters of aromatic compounds (Academic Press, New York, 1973) p. 253.
38 J.R. Lakowicz, H. Cherek, I. Gryczynski, N. Joshi and M.L. Johnson, Biophys. J. 51 (1987) 755.